Ultrasonics 167 (2026) 108190

Contents lists available at ScienceDirect

Ultrasonics

journal homepage: www.elsevier.com/locate/ultras

# Selective assembly of particles using synchronized acoustic tweezers with oblique incidence☆

Yicheng Feng [a], Zhe Zhang [a], Shiyu Li [a,*], Zhixiong Gong [a,b,*]

[a] State Key Laboratory of Ocean Engineering, School of Ocean and Civil Engineering, Shanghai Jiao Tong University, No. 800 Dongchuan Road, Shanghai, 200240, China

[b] Key Laboratory of Marine Intelligent Equipment and System, Ministry of Education, China

ARTICLE INFO

*Keywords:*
Oblique incidence
Synchronized acoustic tweezers
Rayleigh particle
Selective assembly

ABSTRACT

The precise assembly of microparticles and cells shows considerable promise in areas such as bubble–bubble dynamics, reproductive cell selection and fertilization, microchemical reaction measurement, and beyond. Recently, a synchronized acoustic tweezer configuration was theoretically proposed to selectively trap individual particles and subsequently assemble them at a single location [Gong and Baudoin (2019); Gong and Baudoin (2020)]. However, experimental implementation of this method has been limited because the physical overlap of the two acoustic transducers disrupts the effective superposition of the two vortex beams. To address this challenge, we propose an improved design in which the axes of the vortex beams are rotated using oblique incidence. This arrangement ensures (i) effective superposition of the two vortex beams for particle trapping and assembly, and (ii) the feasibility of bringing the two transducers into close proximity without interference. The three-dimensional acoustic radiation forces acting on Rayleigh particles are calculated via Gor'kov potential theory. Numerical simulations performed with different tilt angles of the vortex beams confirm the feasibility of assembling two selectively trapped particles into one spot. This work provides guidance for future experimental designs and demonstrations of particle assembly using acoustic tweezers.

## 1. Introduction

Acoustical tweezers, with the advantage of excellent biocompatibility, and stronger trapping forces than optical tweezers [1–4], have demonstrated splendid ability and prospect in selective trapping of cells and micro-scale particles, which is a critical technique in biomedical and life science, making possible such applications as reproductive cellular selection and mechanical property examination of living cells. Single-beam acoustical tweezers, unlike the acoustical tweezers using standing waves, can be operated with one transducer, better fit for clinical practice [5]. Targeted particles such as cells nevertheless are denser and stiffer than the ambient fluid medium, [6,7], and limits the performance traditional focused beam in selective trapping. The introduction of cylindrical vortices addressed the problem and also provide two-dimensional lateral trapping [3], which offers an insight into the two dimensional particle assembly.

Although acoustic vortex tweezers enable selective particle trapping, the resulting trapping ring tends to repel approaching particles, which impedes multi-particle assembly. This inherent limitation hinders the broader application of the technology in fields like tissue engineering. The repulsive forces exerted by a single acoustic vortex on particles outside its trapping well currently prevent coordinated multi-target assembly. The introduction of synchronized acoustical tweezers [8,9] makes the assembly process possible, as two acoustic vortices destructively interfere with each other and form an attractive path between the two trapped particles to be assembled. However, the research [8] on synchronized acoustical tweezers offers theoretical analysis on the case that the two synchronized acoustical tweezers incident normally on the assembly plane, which leads to the critical problem that the transducers of two tweezers interfere with each other at the end of assembly, making the experimental verification almost impossible. Although Zhang et al. experimentally achieved stable trapping and controlled rotation of morphologically heterogeneous mouse sperm cells using a single spherical vortex tweezer, the manipulation remained two-dimensional. Their results confirmed that a single vortex ring repels particles outside its trapping well [10]. Meanwhile, Ding et al. demonstrated two-dimensional particle assembly using a single-sided ring array to generate multiple off-axis acoustic vortices [11].

☆ This article is part of a Special issue entitled: 'Ultrasonic-Assisted Microfluidics and Streaming' published in Ultrasonics.

* Corresponding authors.
*E-mail addresses:* smwytlsc@sjtu.edu.cn (Y. Feng), the123@sjtu.edu.cn (Z. Zhang), shiyu.li@sjtu.edu.cn (S. Li), zhixiong.gong@sjtu.edu.cn (Z. Gong).

https://doi.org/10.1016/j.ultras.2026.108190
Received 31 January 2026; Received in revised form 10 May 2026; Accepted 7 June 2026
Available online 13 June 2026

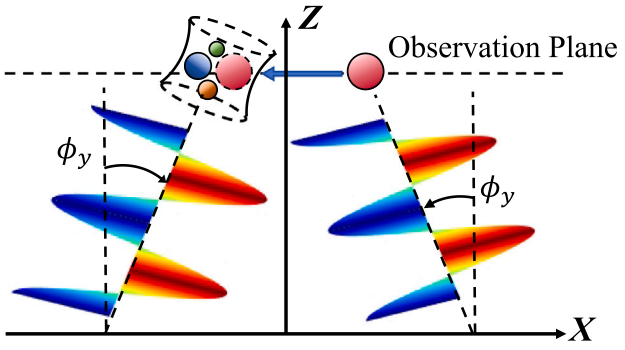


**Fig. 1.** Schematic of two obliquely incident cylindrical Bessel beams used in assembling particles with different properties and size within the Rayleigh regime. $\phi_y$ represents the absolute value of rotation angle in $Y$ direction with the rotation angle of the 1st left beam $\phi_1 = \phi_y$ and the 2nd right beam $\phi_2 = -\phi_y$. The sign of rotation angle $\phi_j (j = 1, 2)$ obeys the right-hand law.

Therefore in this paper we will explore theoretically and numerically the feasibility of two synchronized acoustical tweezers with oblique incidence in particle assembly, as the oblique incidence avoids the interference between two transducers, possibly paving the path to experimental verification. Besides the obliquity can generate an axial radiation force component for Rayleigh particles, since the radiation force generated by normally incident synchronized acoustic tweezers is confined to the plane perpendicular to the beam propagation axis [8].

The paper is organized as follows. Section 2 theoretically analyzed the acoustic field created by cylindrical Bessel beams under oblique incidence, especially the shape and phase of single cylindrical Bessel beam using analytical and numerical methods. In Section 3, we propose the Gor'kov potential method to calculate radiation force. Then theoretically analyzed the Gor'kov potential and radiation force both laterally and axially by single obliquely incident cylindrical Bessel beam with numerical simulation. Also, we give numerical analysis on the case of two obliquely incident vortices with different distance between each center. Finally, we numerically analyzed the critical velocity during assembly. Section 4 reviews the main conclusions and prospect of the paper.

## 2. Acoustic field analysis of cylindrical vortices under oblique incidence

In this section we will consider the interference in a transverse plane of fixed altitude ($z = 0$) between two obliquely incident cylindrical Bessel beams whose respective centers are located in $O_1(-s, 0, 0)$ and $O_2(s, 0, 0)$), with rotation in $Y$ axis respectively as $\phi_y$ and $-\phi_y$. For simplification, define $s_j$ the translation from the original point to center of the $j$th beam(with $s_1 = -s$, $s_2 = s$), and $\phi_j$ the rotation angle in $Y$ direction of the $j$th beam(with $\phi_1 = \phi_y$, $\phi_2 = -\phi_y$), the geometrical relation is displayed in Fig. 2.

Due to the oblique incidence of cylindrical Bessel beam, the transverse plane for observation is not vertical to the axial direction of the Bessel beam, as illustrated in Fig. 1. Thus, the change of amplitude of pressure field and phase along $Z$ axis must be taken into consideration, leading to the radiation force component along axial $Z$ direction in global coordinate system, on which we will later focus on in Section 3.

In this configuration, the pressure field $p_j$ produced by the $j$th vortex ($j = 1$: left vortex; $j = 2$: right vortex) in the coordinate system of the $j$th vortex is given by the equation [3]:

$$p_j = A_j J_m \left(k_\perp r'_j\right) e^{i(m_j \theta'_j + k_\parallel z'_j)} e^{i\beta_j} \tag{1}$$

with $r'_j$ the radial distance with respect to the origin of the $j$th vortex beam in the coordinate system of the $j$th vortex, $z'_j$ the axial distance

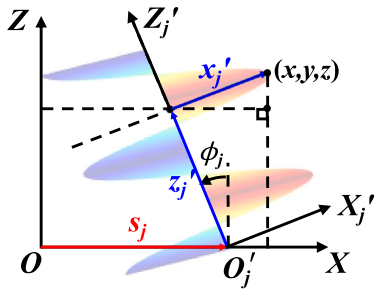


**Fig. 2.** Geometrical relationship of coordinates in local and global coordinate systems of single obliquely incident cylindrical Bessel beam. The local coordinate system is derived from the global coordinate system with the coordinate frame firstly translating along $X$ direction from the global original point $O$ to the center of the $j$th beam $O_j = (s_j, 0, 0)$ and secondly rotating of $\phi_j$ in $Y$ directions, the sign of which is determined by right-hand law.

along the origin of the $j$th vortex beam in the coordinate system of the $j$th vortex, $A_j$ the beam amplitude, $m_j$ its topological charge, $\theta'_j$ the azimuthal phase angle in the coordinate system of the $j$th vortex, and $\beta_j$ the original phase angle, and respectively $k_\perp = k\sin(\gamma)$, $k_\parallel = k\cos(\gamma)$ the transverse and axial wavenumbers, and $k = \omega/c$ the wavenumber, $c$ the sound speed in the fluid, $\omega$ the angular frequency, and $\gamma$ the cone angle.

Note that a cylindrical Bessel beam is completely defined by the topological charge $m$ and the cone angle $\gamma$. Consider vortices of topological order $m = 1$ (Large topological order enlarges the size of the trap well and degrades the trapping stiffness as well as axial forces [8,12,13]. The order is set mostly considered to design acoustical tweezers since it provides the smallest trapping size and stiffest trap.) and $\gamma = 90°$ (leading to $k_\perp = k$ and $k_\parallel = 0$) for simplicity. As previous research has revealed that the in-phase case ($\beta = 0$) is the most suited configuration for particle assembly since it produces the largest and most isotropic rings surrounding the two vortices cores [8], the original phase angle $\beta$ is set $\beta = 0$.

In order to calculate the pressure field of a single obliquely incident cylindrical Bessel beam, introduce the rotation matrix in $Y$ axis as below [14]:

$$R_y(\phi) = \begin{bmatrix} \cos\phi & 0 & -\sin\phi \\ 0 & 1 & 0 \\ \sin\phi & 0 & \cos\phi \end{bmatrix} \tag{2}$$

with $\phi$ the angle of rotation in $Y$ direction, following right-handed law. According to the geometrical illustration in Fig. 2, the relation between the frame of local coordinate system $\left(\hat{x'_j}, \hat{y'_j}, \hat{z'_j}\right)^T$ and global coordinate system $(\hat{x}, \hat{y}, \hat{z})^T$ can be described as $\left(\hat{x'_j}, \hat{y'_j}, \hat{z'_j}\right)^T = R_y(\phi_j)(\hat{x}, \hat{y}, \hat{z})^T$. Therefore the coordinates in local and global systems fall into the equation below.

$$\left(x'_j, y'_j, z'_j\right) \begin{pmatrix} \hat{x'_j} \\ \hat{y'_j} \\ \hat{z'_j} \end{pmatrix} = \left(x - s_j, y, z\right) \begin{pmatrix} \hat{x} \\ \hat{y} \\ \hat{z} \end{pmatrix} \tag{3}$$

Then the relation between coordinates in local and global coordinate systems is derived:

$$\begin{pmatrix} x'_j \\ y'_j \\ z'_j \end{pmatrix} = R_y(\phi_j) \begin{pmatrix} x - s_j \\ y \\ z \end{pmatrix} \tag{4}$$

with $(x'_j, y'_j, z'_j)$ the coordinates in local coordinate system, $(x, y, z)$ in global coordinate system, and $\phi_j$ the rotation angle (with $\phi_1 = \phi_y$, $\phi_2 = -\phi_y$), $s_j$ the origin center of the $j$th Bessel beam (with $s_1 = -s$, $s_2 = s$). The geometrical relation and the generation of local coordinate systems is also shown in Fig. 2.

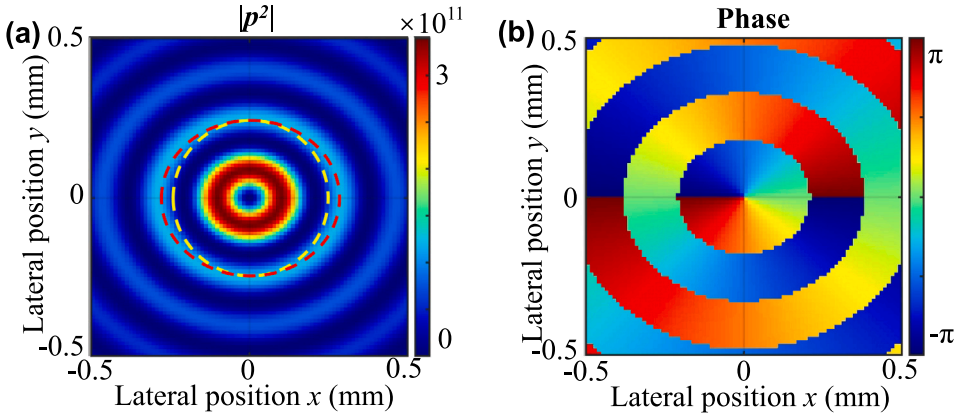


**Fig. 3.** Schematic of cylindrical Bessel beam with oblique incidence of $\phi_y = 30°$ on observe plane $z = 0$. The distance from original point to the center of cylindrical Bessel beam is set $s = 0$ for single cylindrical Bessel beam. (a). Square of the pressure amplitude $|p^2|$ distribution by single cylindrical Bessel beam. The red dashed line shows the shape of pressure field and the yellow dashed line is the perfect circle with respect to the pressure field shape in $Y$ axis. (b). The phase distribution by single cylindrical Bessel beam.

Therefore, the pressure field of single cylindrical Bessel beam is written as following:

$$p_j = A_j J_1(k\tilde{r}_j)e^{i\tilde{\theta}_j} = A_j\left[\frac{J_1(k\tilde{r}_j)}{\tilde{r}_j}(x'_j + y'_j i)\right] \tag{5}$$

with

$$\tilde{r}_j = \sqrt{y^2 + (-z\sin\phi_j + (x - s_j)\cos\phi_j)^2} = \sqrt{x'^2_j + y'^2_j} \tag{6}$$

$$\tilde{\theta}_j = \arg(-z\sin\phi_j + (x - s_j)\cos\phi_j + yi) = \arg(x'_j + y'_j i) \tag{7}$$

The total pressure field created by the interference of two vortices is simply the sum $p = p_1 + p_2$, written as following:

$$p = p_1 + p_2 = A_1\left[\frac{J_1(k\tilde{r}_1)}{\tilde{r}_1}(x'_1 + y'_1 i)\right] + A_2\left[\frac{J_1(k\tilde{r}_2)}{\tilde{r}_2}(x'_2 + y'_2 i)\right] \tag{8}$$

The beam intensity can be quantified with the square of pressure amplitude $|p^2|$ and phase as the argument of the complex pressure field $\arg(p)$. The square of pressure amplitude $|p^2|$ and phase distribution of one cylindrical Bessel beam with incident angle of $\phi_y = 30°$ are illustrated in Fig. 3. The calculation is performed with settings below: the frequency $f = 5$ MHz, the beam amplitudes $A_{1,2} = 10^6$ Pa, and fluid properties of water listed in Table 1 throughout the paper unless specially mentioned. The computational domain is $(x, y, z) \in [-4\lambda, 4\lambda] \times [-4\lambda, 4\lambda] \times [-4\lambda, 4\lambda]$, with $\lambda = 296\,\mu$m.

Unlike the case of vertical incidence, oblique incidence causes the ring-shaped structures of both pressure amplitude squared and phase distribution to become elliptical as shown in Fig. 3. To give theoretical support for the result of elliptical pressure field of single cylindrical Bessel beam oblique incidence on the observe plane $z = 0$, the analysis is given below.

The single cylindrical Bessel beam pressure field is quantified as $|p_j^2|$, and the distribution of pressure field on the observe plane is defined as $|p_j(z = 0)^2| = w_0$, where $w_0$ is a fixed constant, leading to the equation of the curve pressure below:

$$w_0 = |p_j^2| = |A_j J_1(k_\perp \tilde{r}_j(z = 0))|^2 \tag{9}$$

which is equally transformed as such:

$$w\tilde{0}_0 = \tilde{r}_j(z = 0)^2 = \frac{(x - s_i)^2}{1/\cos^2\phi_j} + y^2 \tag{10}$$

Replace the translation along $X$ axis with $\tilde{x} = x - s_j$ in Eq. (10), then the standard ellipse equation can be concluded.

$$1 = \frac{\tilde{x}^2}{(w\tilde{0}_0/\cos\phi_j)^2} + \frac{y^2}{w\tilde{0}_0{}^2} \tag{11}$$

The conclusion of theoretical analysis agrees with the numerical output in Fig. 3(a).

## 3. Radiation force on particles under obliquely incident synchronized vortices

Since single cylindrical Bessel vortex beam does not exert radiation force in the axial direction, the radiation force aroused by single normally incident cylindrical Bessel beam (in such case, $\phi_y = 0$) on Rayleigh particles, is confined within the lateral plane ($z = 0$). However, the oblique incidence rotates the direction of the original axial direction of single cylindrical Bessel beam, leading to an axial component of radiation force along $Z$ axis, which will be discussed later. While the particle assembly with two normally incident synchronized acoustical tweezers has been researched [8], the normal incidence case faces the critical obstacle that the transducers of acoustical tweezers interfere with each other, making it impossible to conduct experiment for verification the theory. Thus the exploration in the pressure field and radiation force arisen by the interference of two obliquely incident synchronized vortex beams avoids the interference of transducers, giving instructions to the experiment of particle assembly.

For this purpose, in this section we will examine the forces exerted on particles trapped at the core of two synchronized acoustical vortices with oblique incidence. By introducing Gor'kov expression [16] of the radiation force in the long wavelength regime, we will compute Gor'kov potential of which radiation force can be expressed as the gradient. Then we can yield the resulting lateral and axial forces (in the $X$ and $Z$ direction) exerted on two particles trapped at the center of two cylindrical acoustical vortices with oblique incidence during the assembly process.

First consider polystyrene (PS) particles of small radius $a = 5$ μm compared to the wavelength $\lambda = 296\,\mu$m, in the range of validity of Gor'kov theory ($ka \approx 1/10 \ll 1$). These particles are chosen to demonstrate that particle assembly is possible with this method even for low acoustical contrast with the surrounding fluid (with acoustic property parameters listed in Table 1). Following Gor'kov [16], the radiation force $\mathbf{F}$ can be expressed as the negative gradient of the potential $U$,

$$\mathbf{F} = -\nabla U \tag{12}$$

with:

$$U = 2\pi a^3 \rho_0 \left(\frac{\langle p^2\rangle}{3\rho_0^2 c_0^2} f_1 - \frac{\langle \mathbf{v}^2\rangle}{2} f_2\right), \tag{13}$$

and $f_1 = 1 - \tilde{\kappa}$ (with the compressibility ratio $\tilde{\kappa} = \kappa_p/\kappa_0$, and $\kappa_p$ the compression rate of PS particle and $\kappa_0$ of water) and $f_2 = 2(\tilde{\rho} - 1)/(2\tilde{\rho} + 1)$ (with density ratio $\tilde{\rho} = \rho_p/\rho_0$, and $\rho_p$ the density of PS particle and $\rho_0$ of water) are the respective contributions of the monopolar and

**Table 1**
Acoustic properties of the fluid and the material of particles (polystyrene, PS) in three scenarios with density ($\rho$), longitudinal sound speed ($c$), and compression rate ($\kappa$), which are extracted from [15].

| Material | Density $\rho$ (kg/m$^3$) | Speed of sound $c$ (m/s) | Compression rate $\kappa$ (1/TPa) |
|---|---|---|---|
| water | 998.2 | 1482 | 456 |
| polystyrene | 1050 | 2350 | 172 |

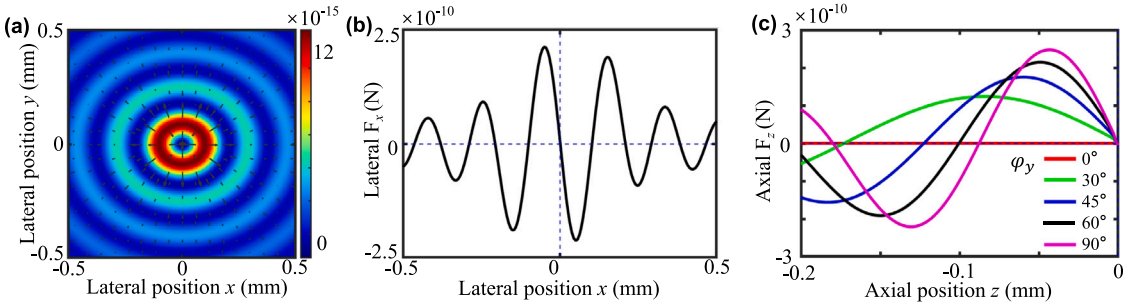


**Fig. 4.** Schematic of single cylindrical Bessel beam with oblique incidence and radiation force on PS spheres of 5 μm. The distance from original point to the center of cylindrical Bessel beam is set $s = 0$ for single cylindrical Bessel beam. (a). Gor'kov potential (color) and radiation force (arrows) with incident angle $\phi_y = 30°$ on observe plane $z = 0$. (b). Lateral force $F_x$ (in newton) exerted on the particle as function of $x$(in mm) with incident angle $\phi = 30°$. (c). Axial force $F_z$ (in newton) exerted on the particle as function of $z$(in mm) with incident angle $\phi_y = 0°, 30°, 45°, 60°, 90°$.

dipolar vibrations of the particle [17]. The value of these factors are listed in Table 1. $p$ and $\mathbf{v}$ are the pressure and velocity associated with the total incident acoustic field in the fluid. Note that the expression of $f_1$ in Gor'kov's original paper [16] based solely on the longitudinal velocity inside the particle only applies for liquid spheres. The velocity vector is related to the complex pressure, as $\mathbf{v} = -i/(\rho_0\omega)\nabla p$. To yield the velocity vector, first calculate the gradient of the complex pressure field.

$$\nabla p_j = \begin{pmatrix} \partial_x p_j \\ \partial_y p_j \\ \partial_z p_j \end{pmatrix} = R_y^T(\phi_j) \begin{pmatrix} \partial_{x'} p_j \\ \partial_{y'} p_j \\ \partial_{z'} p_j \end{pmatrix} \tag{14}$$

where $\partial_x = \partial/\partial x$ as $\partial_x, \partial_y, \partial_z, \partial_{x'}, \partial_{y'}, \partial_{z'}$ similarly defined, with the superscript noting the local system and subscript $j$ omitted in this part. Eq. (14) can be directly derived from Eq. (4), the Jacobian determinant. Therefore, detailed calculation comes the following.

$$\partial_{x'} p_j = A_j \left( \frac{J_1(k\tilde{r_j})}{\tilde{r_j}} - \frac{k(x_j' + iy_j')x_j' J_2(k\tilde{r_j})}{\tilde{r_j}^2} \right) \tag{15}$$

$$\partial_{y'} p_j = A_j \left( \frac{iJ_1(k\tilde{r_j})}{\tilde{r_j}} - \frac{k(x_j' + iy_j')y_j' J_2(k\tilde{r_j})}{\tilde{r_j}^2} \right) \tag{16}$$

$$\partial_{z'} p_j = 0 \tag{17}$$

thus yielding the expression of velocity vector.

$$\mathbf{v}_j = -\frac{i}{\rho_0\omega}\nabla p_j = -\frac{i}{\rho_0\omega} R_y^T(\phi_j) \begin{pmatrix} \partial_{x'} p_j \\ \partial_{y'} p_j \\ \partial_{z'} p_j \end{pmatrix} \tag{18}$$

In expression Eq. (18), substitute local coordinates with global coordinates using the coordinate transformation equation Eq. (4). Hence the time average of $\langle p_j^2 \rangle$ and $\langle \mathbf{v}_j^2 \rangle$ in the global coordinate system come as following:

$$\langle p_j^2 \rangle = \frac{1}{2}\mathrm{Re}(p_j p_j^*) \tag{19}$$

$$\langle \mathbf{v}_j^2 \rangle = \frac{1}{2}\mathrm{Re}(\mathbf{v}_j^\dagger \mathbf{v}_j) \tag{20}$$

where $p_j^*$ is the complex conjugate of $p_j$ and $\mathbf{v}_j^\dagger$ is the Hermitian transpose of $\mathbf{v}_j$, then substitute the result into Eqs. (12) and (13), yielding the numerical output as illustrated in Fig. 4.

The result of Gor'kov potential and radiation force created by single cylindrical Bessel beam in Fig. 4(a) shows that the shape of Gor'kov potential agrees with that of pressure field, with a distinctive elliptical distortion, making the scale of potential trap laterally in $X$ axis (in this case) wider, and correspondingly weakening the maximum value of radiation force along the assembly direction ($X$ axis). Nevertheless, the radiation force in $X$ axis ($F_x$) still holds a stiff well trap at the central and equilibrium position as shown in Fig. 4(b) . Furthermore, the reduction in $F_x$ caused by obliquity gives rise to radiation force in $Z$ axis. As Fig. 4(c) shows a positive correlation between incident angle $\phi_y$ and the maximum of $F_z$, with the maximum of $F_z$ comes to extremum at $\phi_y = 90°$, which is simply the lateral radiation force at the core position in normally incident case. This gives an insight that two synchronized vortices with oblique incidence when assembling particles may additionally provide axial ($Z$ axis) well trap during the process of assembly at the cost of a weakened lateral radiation force $F_x$.

Actually, the relation between $F_x$ and $F_z$ can be quantified as below.

$$F_x = -\frac{\partial}{\partial x}U = -\nabla' \cdot \frac{\partial}{\partial x}\begin{pmatrix} x' \\ y' \\ z' \end{pmatrix} U = -\cos\phi \frac{\partial}{\partial x'}U = F_{x'}\cos\phi \tag{21}$$

$$F_z = -\frac{\partial}{\partial z}U = -\nabla' \cdot \frac{\partial}{\partial z}\begin{pmatrix} x' \\ y' \\ z' \end{pmatrix} U = \sin\phi \frac{\partial}{\partial x'}U = -F_{x'}\sin\phi \tag{22}$$

with $\partial U/\partial z' = 0$, consistent with that cylindrical Bessel beam has zero gradient in propagation axis. $\nabla' = (\partial/\partial x', \partial/\partial y', \partial/\partial z')^T$, and $F_{x'}$ is the lateral radiation force in the local system and equally the normally incident case, and $\phi$ is the incident angle with subscript $j$ omitted for simplification. The theoretical analysis agrees with the result in Fig. 4 and the discussion above.

In the two vortices case, the Gor'kov potential and radiation force follow the similar form with:

$$\langle p^2 \rangle = \frac{1}{2}pp^*, \quad p = p_1 + p_2 \tag{23}$$

$$\langle \mathbf{v}^2 \rangle = \frac{1}{2}\mathbf{v}^\dagger \mathbf{v}, \quad \mathbf{v} = \mathbf{v}_1 + \mathbf{v}_2 \tag{24}$$

then calculate the corresponding Gor'kov potential and radiation force with different distance between two vortices, the result is shown in Fig. 5.

These figures show that particles can still be trapped separately in the two vortices, when the static equilibrium positions (zero force) are located in the region of negative forces gradient, with the restoring forces pushing them back to the equilibrium positions. A clear assembly

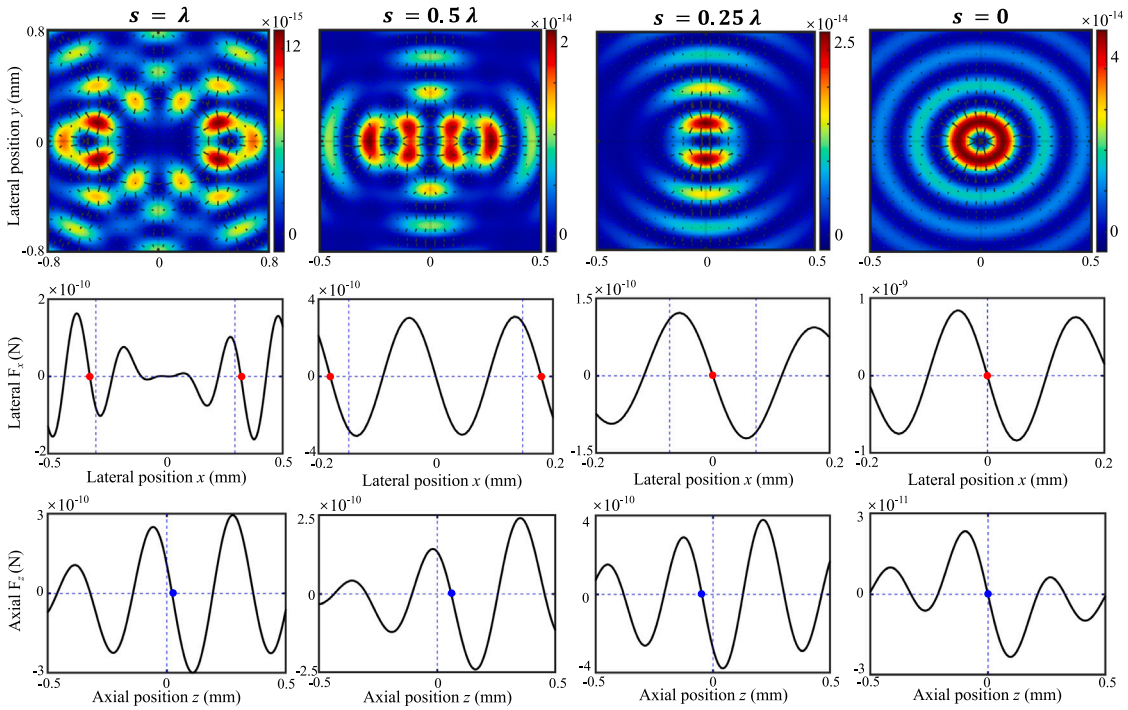


**Fig. 5.** Schematic of synchronized acoustical tweezers with particle assembly with incident angle $\phi_y = 30°$. The column from left to right displays spatial relation $s = \lambda, 0.5\lambda, 0.25\lambda, 0$, the distance between the center of each vortex and the global original point, and $\lambda$ the wavelength. Row 1: the Gor'kov potential (color) and radiation force (arrow). Row 2: the radiation force along $X$ axis at $y = 0, z = 0$, with vertical dashed lines the core of each vortex and horizontal dashed line $F_x = 0$, and red dots the static equilibrium positions in $X$ direction. Row 3: the radiation force along $Z$ axis at $x = s, y = 0$, the center of the right vortex, with vertical dashed line $z = 0$ and horizontal dashed line $F_z = 0$, and blue dots the static equilibrium positions in $Z$ direction.

path created by destructive interference is displayed. Note that the static equilibrium positions (marked in red dots) differ from the position of the individual vortex cares (displayed with vertical dashed lines in Fig. 5 row 2), due to the interference between the two vortices. In Fig. 5 row 3 shows the quasi-static analysis of the axial force $F_z$, at the center of each vortex, the equilibrium positions (marked in blue dots) tend to fluctuate around the $z = 0$ plane, but generally form a well trap in $Z$ direction during the whole process. However, during the dynamic assembly process, the axial force tend to push away particles from the observation plane $z = 0$. To realize assembly, a physical restrain need to be applied to restrict target particles to the assembly and observe plane. At the final stage of assembly, there forms a 3D well trap around the core of each vortex, as is shown in Fig. 5.

While in practice, particles must be moved with a finite velocity, which leads to the existence of a drag force applied by the fluid on the particles. This drag force can expel the particle from the trap if the radiation force is not sufficient to counteract it. Previous research on two normally incident vortices has given the speed limit at which two particles can be assembled [8], with the assumption that (i) the particles are moved by the tweezers at a constant velocity $v_{cr}$ and (ii) the flow around the particles is in the low Reynolds regime ($Re \ll 1$). Considering the small size of the particles ($a = 5$ μm), this assumption holds for particles velocities: $v_{cr} \ll \eta/\rho a = 0.2$ ms$^{-1}$ in water, with $\eta$ the fluid dynamic viscosity. This value is several orders of magnitude larger than the typical velocities used for microparticles manipulation and thus, the low Reynolds hypothesis is consistent. And thus the drag force is simply the Stokes drag: $F_d = 6\pi\eta a v_{cr}$, leading to the expression of critical velocity [8].

$$v_{cr} = F_x^{\text{peak}}/6\pi\eta a. \tag{25}$$

where $F_x^{\text{peak}}$ is the closest maximum value of lateral radiation force $F_x$ to the equilibrium positions.

Through numerical simulation, in the oblique incidence case (with incident angle $\phi_y = 30°$), the minimum $F_x^{\text{peak}}$ occurs at $s/\lambda = 0.3$, where $F_x^{\text{peak}} \approx 3 \times 10^{-11}$ N, which is close to the result of normally incident case [8]. The result is displayed in Fig. 6(a). Therefore, within the critical velocity, the particle can be successively moved and then brought to a single centered trap, when the two vortex beams approach each other.

Furthermore, to evaluate the capability of assembly with different incident angles $\phi_y$, numerical analysis is conducted. Assembly capability is measured by minimum lateral radiation force $F_x$ near each vortex center during the assembly process. The result in Fig. 6(b) shows that as the incident angle increases, the assembly capability goes through slight enhancement and then decreases to zero.

## 4. Conclusion and outlook

In this paper, we have theoretically demonstrated the feasibility of using two synchronized cylindrical vortex beams with oblique incidence to transport and assemble particles much smaller than the wavelength. The introduction of oblique incidence gives rise to an axial radiation force component, effectively creating a three-dimensional trapping potential in quasi-static scenarios. We have also numerically analyzed and quantified the assembly capability across different incident angles, showing that the lateral trapping stiffness can be maintained or even slightly enhanced over a useful angular range.

Future work can be pursued in two main directions. From the point of the view of theory, general theories are in need. The current analysis relies on the Gor'kov potential, which is valid only in the Rayleigh regime ($ka \ll 1$). To generalize the method to larger particles and dense clusters where inter-particle coupling becomes significant, future work will employ the angular spectrum method (ASM) or multipole expansion method (MEM) in conjunction with T-matrix formulations and full multiple-scattering theory [18–23]. This will establish a theoretical model that rigorously accounts for particle–particle acoustic interactions, enabling the evaluation of whether the interference-mediated

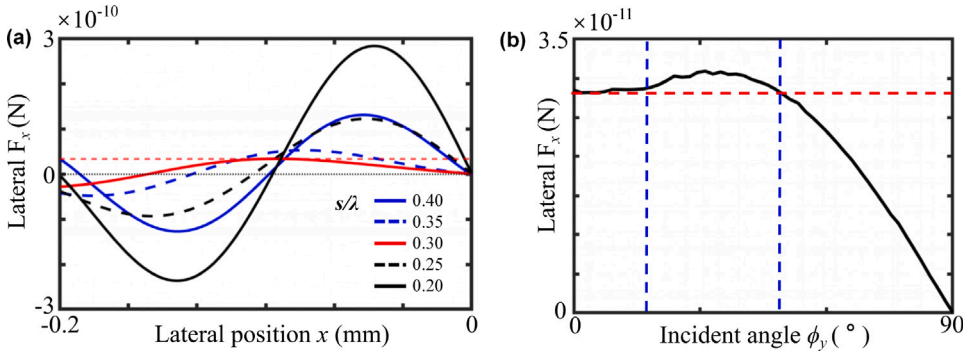


**Fig. 6.** (a). Lateral radiation force $F_x$ (in Newton) applied on PS spheres in water by two obliquely incident interfering vortex beams with distance between vortex core to global original point from $s/\lambda = 0.4$ to $s/\lambda = 0.2$. The zero point of $x$ is set the nearest equilibrium point from the left vortex center, changing with $s$. The graph only shows the force for particles located in the half plane $x < 0$ on the $X$ axis. Results for particles located in the half plane $x > 0$ can be inferred from these data by simple symmetry. The red dashed line describes the critical radiation force at $s/\lambda = 0.3$ which is balanced by the Stokes drag force to determine the critical velocity $v_{cr}$ of the moving tweezers. (b). Assembly capability is measured by the minimum lateral radiation force $F_x$ near each vortex center during the assembly process versus the oblique incidence angle $\phi_y$ ($0° \le \phi_y \le 90°$). For each $\phi_y$, the synchronized approach of the two vortices is simulated from an initial center separation $s = 2\lambda$ to $s = 0$. Red dashed line marks the area that the assembly capability start to decrease, and blue dashed lines demonstrates the range of $\phi_y$ where the assembly capability is enhanced.

assembly pathways identified here remain applicable in complex biological systems. From the point of view of the experiment, the proposed scheme can be realized by mounting the two transducers on precision motorized stages and gradually reducing their lateral separation while keeping the tilt angle $\phi_y$ fixed. The main practical constraint is the finite aperture of the ultrasonic transducers. The physical interference of the transducers sets a lower and upper bound on the feasible tilt angle. Fig. 6(b) shows that this bound should lie well within the angular range where the assembly capability is preserved or even enhanced. The use of smaller transducers would further relax this geometric restriction. Moreover, an intriguing extension would be to apply the oblique-incidence scheme to synchronized spherical acoustic vortices [10,24]. Since spherical vortex transducers have already been fabricated and tested, combining them with the tilted configuration discussed here could pave the path to three-dimensional dynamic assembly that is not achievable with cylindrical vortices alone.

## CRediT authorship contribution statement

**Yicheng Feng:** Writing – review & editing, Writing – original draft, Data curation, Conceptualization. **Zhe Zhang:** Writing – review & editing, Data curation. **Shiyu Li:** Writing – review & editing, Validation, Resources, Project administration, Methodology, Conceptualization. **Zhixiong Gong:** Writing – review & editing, Methodology, Funding acquisition, Conceptualization.

## Declaration of competing interest

The authors declare that they have no known competing financial interests or personal relationships that could have appeared to influence the work reported in this paper.

## Acknowledgments

Z. Gong thanks for the support from the National Natural Science Foundation of China (24Z990200542 and No. 12504522), the XIAOMI Foundation, and the Shanghai Jiao Tong University [2030 Initiative, AI for Engineering Initiative, and the startup funding (WH220401017, WH22040121)].

## Appendix A. Supplementary data

Supplementary material related to this article can be found online at https://doi.org/10.1016/j.ultras.2026.108190.

## Data availability

Data will be made available on request.

## References

[1] A. Ozcelik, J. Rufo, F. Guo, Y. Gu, P. Li, J. Lata, T.J. Huang, Acoustic tweezers for the life sciences, Nature Methods 15 (12) (2018) 1021–1028.
[2] M. Baudoin, J.-L. Thomas, R.A. Sahely, J.-C. Gerbedoen, Z. Gong, A. Sivery, O.B. Matar, N. Smagin, P. Favreau, A. Vlandas, Spatially selective manipulation of cells with single-beam acoustical tweezers, Nat. Commun. 11 (1) (2020) 4244.
[3] M. Baudoin, J.-L. Thomas, Acoustic tweezers for particle and fluid micromanipulation, Annu. Rev. Fluid Mech. 52 (1) (2020) 205–234.
[4] K. Dholakia, B.W. Drinkwater, M. Ritsch-Marte, Comparing acoustic and optical forces for biomedical research, Nat. Rev. Phys. 2 (9) (2020) 480–491.
[5] S. Li, L. Chen, Y. Feng, X. Cheng, Z. Gong, A review on single-beam acoustical tweezers: From tractor beam to selective trapping, Ultrasonics 165 (2026) 108061.
[6] Z. Gong, M. Baudoin, Single beam acoustical tweezers based on focused beams: A numerical analysis of two-dimensional and three-dimensional trapping capabilities, Phys. Rev. Appl. 18 (4) (2022) 044033.
[7] S. Li, Z. Gong, Reversing the acoustic contrast factor by tuning the medium can make focused beams trap cells in three dimensions, Phys. Fluids 37 (1) (2025).
[8] Z. Gong, M. Baudoin, Particle assembly with synchronized acoustic tweezers, Phys. Rev. Appl. 12 (2) (2019) 024045.
[9] Z. Gong, M. Baudoin, Three-dimensional trapping and assembly of small particles with synchronized spherical acoustical vortices, Phys. Rev. Appl. 14 (6) (2020) 064002.
[10] T. Zhang, Y. Huang, Z. Xu, K. He, Z. Wang, H. Hang, X. Zhou, G. Yu, J. Ou-Yang, X. Yang, F. Wang, B. Zhu, Precise capture of heterogeneous microscale targets using an integrated spherical vortex acoustic tweezer, Ultrasonics 165 (2026) 108083.
[11] N. Ding, G. Guo, J. Tu, D. Zhang, Q. Ma, Two-dimensional particle assembly based on the synchronized evolution of centrosymmetric off-axis acoustic vortexes, Engineering 47 (2025) 139–151.
[12] A. Crivoi, J. Tai, X. Ji, Z. Fan, Scaling acoustic vortex traps with topological charge, Ultrasonics 155 (2025) 107710.
[13] P.L. Marston, Scattering of a Bessel beam by a sphere: II. Helicoidal case and spherical shell example, J. Acoust. Soc. Am. 124 (5) (2008) 2905–2910.
[14] G.B. Arfken, H.J. Weber, F.E. Harris, Rotations in $\mathbb{R}^3$, in: Mathematical Methods for Physicists, seventh ed., Academic Press, 2013, pp. 139–141.
[15] M. Settnes, H. Bruus, Forces acting on a small particle in an acoustical field in a viscous fluid, Phys. Rev. E 85 (1) (2012) 016327.
[16] L. Gor'kov, On the forces acting on a small particle in an acoustical field 49. in an ideal fluid, Sov. Phys. Dokl. 6 (1962) 773–775.
[17] H. Bruus, Acoustofluidics 7: The acoustic radiation force on small particles, Lab Chip 12 (6) (2012) 1014–1021.
[18] Z. Gong, L.P. Marston, W. Li, Y. Chai, Multipole expansion of acoustical bessel beams with arbitrary order and location, J. Acoust. Soc. Am. 141 (6) (2017) EL574–EL578.

[19] Z. Gong, P.L. Marston, W. Li, T-matrix evaluation of three-dimensional acoustic radiation forces on nonspherical objects in bessel beams with arbitrary order and location, Phys. Rev. E 99 (6) (2019) 063004.
[20] S. Li, Z. Gong, Combined effect of acoustic radiation force and acoustic streaming for focused beams to trap cells in three dimensions, J. Acoust. Soc. Am. 156 (4_Supplement) (2024) A43.
[21] J.H. Lopes, M. Azarpeyvand, G.T. Silva, Acoustic interaction forces and torques acting on suspended spheres in an ideal fluid, IEEE Trans. Ultrason. Ferroelectr. Freq. Control 63 (1) (2016) 186–197.
[22] T. Tang, L. Huang, Acoustic radiation force for multiple particles over a wide size-scale by multiple ultrasound sources, J. Sound Vib. 509 (2021) 116256.
[23] T. Tang, L. Huang, Mie particle assembly by a converging ultrasound field and acoustic interaction forces, Appl. Acoust. 180 (2021) 108123.
[24] S. Li, Y. Feng, W. Cui, Z. Gong, Experimental demonstration for precisely tuning the focal length of finite-aperture focused beams and vortex, 2026, arXiv:2604.12595.